IMMEDIATE COMMUNICATION

Check for updates

Cylindromatosis drives synapse pruning and weakening by promoting macroautophagy through Akt-mTOR signaling

Alexis S. Zajicek[1,2], Hongyu Ruan[1], Huihui Dai[1], Mary C. Skolfield [1,2], Hannah L. Phillips[1,2], Wendi J. Burnette[1,2], Behnam Javidfar[3], Shao-Cong Sun[4], Schahram Akbarian [3] and Wei-Dong Yao [1,2,5,6,7 ✉]

The lysine-63 deubiquitinase cylindromatosis (CYLD) is long recognized as a tumor suppressor in immunity and inflammation, and its loss-of-function mutations lead to familial cylindromatosis. However, recent studies reveal that CYLD is enriched in mammalian brain postsynaptic densities, and a gain-of-function mutation causes frontotemporal dementia (FTD), suggesting critical roles at excitatory synapses. Here we report that CYLD drives synapse elimination and weakening by acting on the Akt-mTOR-autophagy axis. Mice lacking CYLD display abnormal sociability, anxiety- and depression-like behaviors, and cognitive inflexibility. These behavioral impairments are accompanied by excessive synapse numbers, increased postsynaptic efficacy, augmented synaptic summation, and impaired NMDA receptor-dependent hippocampal long-term depression (LTD). Exogenous expression of CYLD results in removal of established dendritic spines from mature neurons in a deubiquitinase activity-dependent manner. In search of underlying molecular mechanisms, we find that CYLD knockout mice display marked overactivation of Akt and mTOR and reduced autophagic flux, and conversely, CYLD overexpression potently suppresses Akt and mTOR activity and promotes autophagy. Consequently, abrogating the Akt-mTOR-autophagy signaling pathway abolishes CYLD-induced spine loss, whereas enhancing autophagy in vivo by the mTOR inhibitor rapamycin rescues the synaptic pruning and LTD deficits in mutant mice. Our findings establish CYLD, via Akt-mTOR signaling, as a synaptic autophagy activator that exerts critical modulations on synapse maintenance, function, and plasticity.

INTRODUCTION

The tumor suppressor *CYLD* encodes a lysine-63 (K63) deubiquitinating enzyme (DUB) [1] and its loss-of-function mutations cause familial cylindromatosis, an autosomal dominant predisposition to head and neck skin tumors [2]. Unlike lysine-48 (K48)-linked polyubiquitin chains that tag protein substrates for proteasomal degradation, K63 chains facilitate multiprotein complex assembly during signaling transduction, and are classically involved in the NF-κB pathway that mediates immune response and inflammation [3, 4]. Landmark studies have established that CYLD suppresses tumorigenesis and promotes apoptosis by cleaving K63 chains on key components of the NF-κB pathway, inhibiting NF-κB activation [5–7]. CYLD also negatively regulates other processes, such as TGFβ signaling via deubiquitinating its substrate Akt/PKB [8]. Mice deficient in CYLD display modest immune phenotypes, as they do not develop tumors spontaneously but show increased susceptibility to tumorigenesis and other immune deficits when challenged [9–11].

CYLD is rapidly emerging as a major player at synapses in the mammalian brain [12]. CYLD is enriched in the postsynaptic density (PSD) of excitatory synapses [13, 14], is recruited to the PSD in response to activity [15], and interacts with >100 synaptic proteins in mouse striatal synaptosomes [16]. CYLD deubiquitinates and regulates synaptic abundance of the postsynaptic scaffold PSD-95, regulates synaptic strength, and mediates NMDA receptor (NMDAR)-dependent chemical LTD (cLTD) in cultured neurons [14]. Although most heavily enriched in the PSD, CYLD is also present in the presynaptic fraction of rodent brain [14] and regulates axonal length in cultured mouse hippocampal neurons [17]. In addition, CYLD has a role in inhibitory synaptic transmission and regulates GABA receptor trafficking/turnover in striatal neurons [18]. CYLD deficiency is associated with anxiety-like and autism behaviors [19, 20]. Finally, a gain-of-function mutation and variants of *CYLD* were identified in patients with frontotemporal dementia (FTD)/amyotrophic lateral sclerosis (ALS) [17, 21], placing *CYLD* as the newest member of the FTD/ALS gene family. However, the precise role of CYLD in synaptic remodeling, plasticity, and behavior in vivo remains poorly understood.

Macroautophagy (autophagy) is a conserved catabolic process that delivers unnecessary or damaged cytosolic constituents to lysosomes for degradation to maintain cellular homeostasis [22, 23]. Autophagy is particularly important in neurons, which

[1]Department of Psychiatry and Behavioral Sciences, State University of New York, Upstate Medical University, Syracuse, NY 13210, USA. [2]Neuroscience Graduate Program, State University of New York, Upstate Medical University, Syracuse, NY 13210, USA. [3]Friedman Brain Institute, Department of Psychiatry, Icahn School of Medicine at Mount Sinai, New York, NY 10029, USA. [4]Department of Immunology, University of Texas MD Anderson Cancer Center, Houston, TX, USA. [5]Department of Neuroscience and Physiology, State University of New York, Upstate Medical University, Syracuse, NY 13210, USA. [6]Harvard Medical School, New England Primate Research Center, Southborough, MA, USA. [7]Department of Psychiatry, Beth Israel Deaconess Medical Center, Boston, MA, USA. ✉email: yaow@upstate.edu
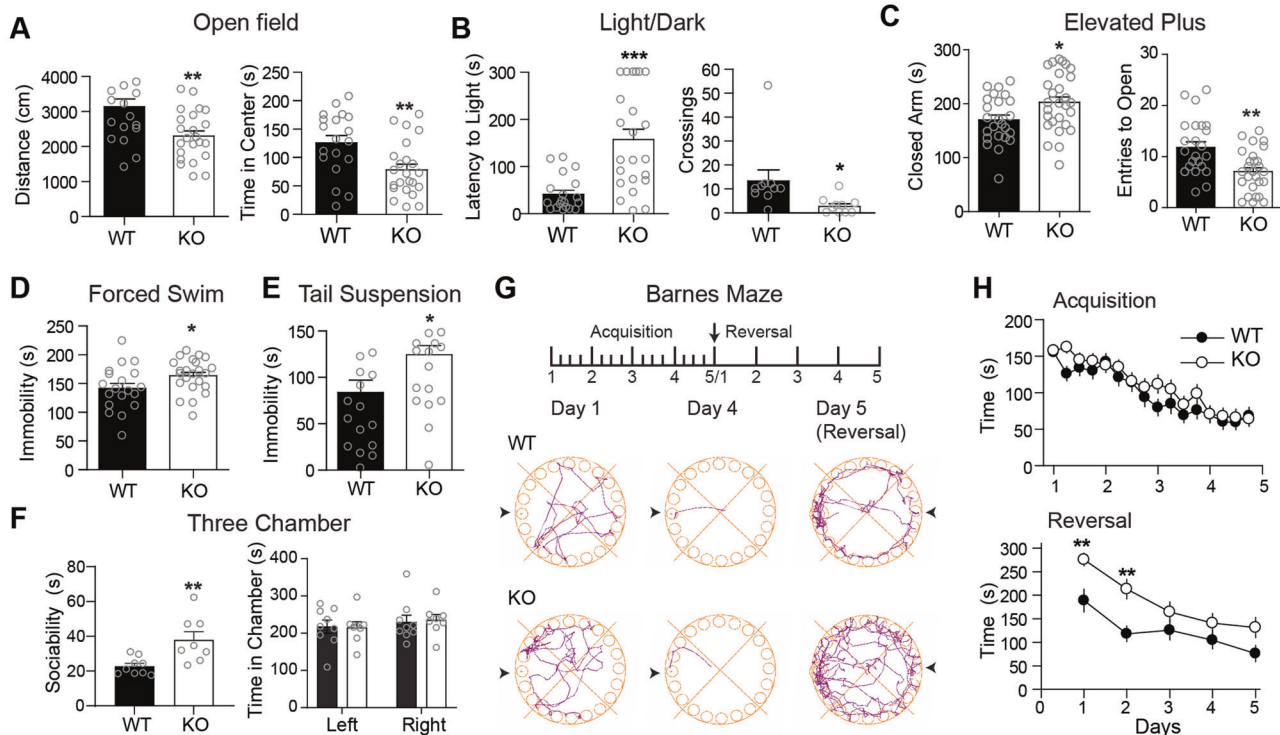
Fig. 1 Aberrant locomotor, social, affective, and cognitive behaviors in CYLD KO mice. A Open field test. **B** Light/Dark test. **C** Elevated plus maze test. **D** Forced-swim test. **E** Tail-suspension test. **F** Three-chamber sociability test. **G** Experimental timeline and representative track plots from mice during a Barnes maze test. Arrowheads represent current location of the escape tunnel. **H** Barnes maze quantifications. Time represents latency to escape during a 3-min test four times daily (top) or a 5-min single trial each day during reversal (bottom). $n = 19$ (WT) and 23 (KO) mice for **A–D**; $n = 15$ (WT) and 15 (KO) mice for **E**; $n = 8$ (WT) and 9 (KO) mice for **F**; $n = 30$ (WT) and 33 (KO) mice for (**H**). *$p < 0.05$; **$p < 0.01$; ***$p < 0.001$. Two-tailed unpaired *t*-tests, Mann-Whitney U test, or two-way ANOVA with Bonferroni's multiple comparison test. Summary data are mean ± sem.

are postmitotic and must thrive throughout an organism's lifetime. Indeed, autophagy plays essential roles in neuron viability and development [24, 25] and is implicated in numerous neurodegenerative and psychiatric diseases [26–30]. Increasing evidence also supports critical roles for neuronal autophagy in synaptic function, remodeling, and plasticity [31–33]. In particular, neuronal autophagy is induced during, and required for, NMDAR-dependent LTD [34–36], and autophagy induction promotes hippocampal long-term potentiation (LTP) and memory formation and reverses age-related memory decline [37]. Furthermore, neuronal autophagy promotes synapse pruning in human and mouse cortex during adolescent development [38]. mTOR, a multipurpose serine/threonine kinase localized in the synapse, is a central regulator of autophagy. Together with its upstream activator Akt, mTOR inhibits autophagosome formation, the induction step of autophagy [39, 40]. Impaired mTOR-autophagy is involved in aberrant synaptic pruning associated with autism [38] and synaptic and cognitive deficits in a mouse model of fragile X syndrome [41].

In this study, we show that CYLD drives synapse pruning, weakens synaptic strength, and mediates LTD by stimulating Akt-mTOR-autophagy signaling, and is required for maintenance of social, affective, and cognitive behaviors.

MATERIALS AND METHODS
All procedures involving animals were approved by the SUNY Upstate Medical University or the Icahn School of Medicine at Mount Sinai Institutional Animal Care and Use Committees. Please see Supplementary Methods for details on animals, reagents, cell cultures, viruses, stereotaxic surgery, immunohistochemistry, biochemistry, confocal microscopy and imaging analysis, electrophysiology, and behavioral assays.

All data is represented as mean ± SEM. Details on statistic tests, justifications, sample sizes, and p-values are presented in figure legends and Supplementary Methods. No data was excluded from analysis. Mice and drug treatments were randomly assigned to each genotype or group. Significance threshold was set at $p = 0.05$. All statistical analyses were performed using Prism 7 (GraphPad).

RESULTS
Aberrant social, affective, and cognitive behaviors in CYLD-deficient mice
To gain initial insights into in vivo roles of CYLD in the brain, we subjected CYLD WT and KO mice to a battery of behavioral tests (Fig. 1). CYLD KO mice travelled significantly less distance and spent less time in the center of an open field compared to WT littermates (Fig. 1A), suggesting impaired locomotor activity and/or reduced motivation to explore, as well as increased anxiety-like behavior. KO mice displayed longer latency and fewer crossings to light in a Light/Dark box (Fig. 1B) and spent more time in the closed arms and had fewer entries to the open arms in an elevated plus maze (Fig. 1C), signaling heightened anxiety. KO mice showed significant increases in the duration of immobility than WT in both forced swim and tail suspension tests (Fig. 1D, E), suggesting a depression-like phenotype. CYLD KO mice spent significantly more time interacting with a stranger conspecific compared to WT, though the time in each chamber remained unchanged, suggesting increased sociability (Fig. 1F). Working memory appeared unaltered in KO mice as they showed similar spontaneous alternations to WT in a Y-maze (Fig. S1A, B). Finally, when placed in a Barnes maze, KO mice spent a similar amount of time as WT mice (Fig. 1G, H) and even made fewer errors when learning to find an escape tunnel (Fig. S1C), suggesting an equal
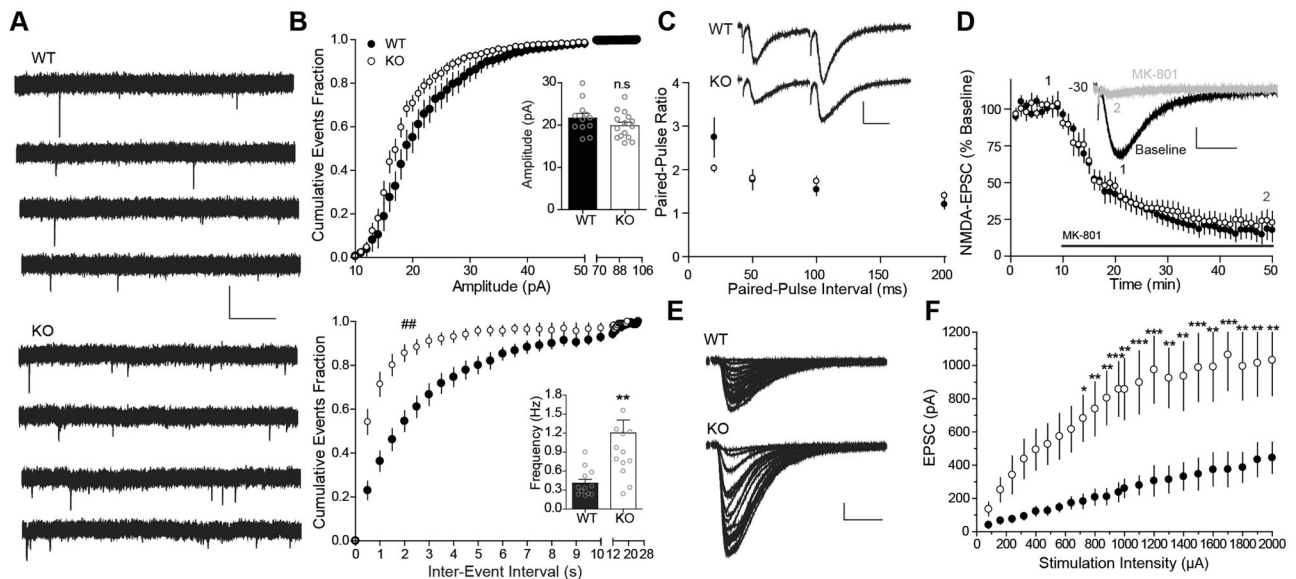
Fig. 2 Enhanced postsynaptic efficacy in CYLD KO mice. A Representative mEPSC traces from CA1 hippocampal neurons. Scale bar: 40 pA, 2 sec. **B** Cumulative probability distributions of mEPSC amplitude and inter-event intervals. Insets, Mean amplitudes and frequencies. $n = 12$ (WT) and 15 (KO) cells. $^{##}p < 0.01$, Kolmogorov–Smirnov test; $^{**}p < 0.01$; n.s., not significant; two-tailed unpaired t-tests. **C** Paired-pulse ratio. Scale bar: 100 pA, 20 ms. $n = 8$ (WT) and 8 (KO) cells. Not significant by two-way ANOVA with Bonferroni's multiple comparison test. **D** MK-801 assay. NMDA-EPSCs before and after MK-801 (20 μM) wash-in were recorded at −30 mV. Inset, representative NMDA-EPSC before (1) and after (2) MK-801. Scale bar: 100 pA, 50 ms. $n = 6$ (WT) and 6 (KO) cells. **E, F** Representative (**E**) and summary (**F**) EPSCs in response to varying stimulation intensities at Schaffer collateral-CA1 synapses. Scale bar: 200 pA, 20 ms. $n = 16$ (WT) and 10 (KO) cells. $^*p < 0.05$, $^{**}p < 0.01$, $^{***}p < 0.001$. Two-way ANOVA with Bonferroni's multiple comparisons test. Summary data are mean ± sem.

or better performance during initial acquisition. However, KO mice had difficulty in re-learning the escape tunnel when it was in the opposite location, especially during first two days of the reversal learning test (Fig. 1G, H), primarily due to longer time spent near the previous tunnel location, longer time taken to locate the new escape tunnel, and an altered search strategy (Fig. S1D–I). These results suggest impaired cognitive flexibility in CYLD KO mice.

Enhanced postsynaptic efficacy in CYLD KO mice
We next performed whole-cell patch-clamp analyses on hippocampal CA1 and medial prefrontal cortex (mFC) layer 5 pyramidal neurons in slices prepared from WT and KO mice (Fig. 2). In CA1 (P20-P30), the frequency of AMPA receptor (AMPAR)-mediated miniature excitatory postsynaptic currents (mEPSCs) was significantly higher in KO neurons compared to WT with the mEPSC amplitude being indistinguishable between the two groups (Fig. 2A, B), suggesting an increase in presynaptic glutamate release probability and/or number of functional synapses in mutant neurons. In mPFC, mEPSC frequency was also significantly higher in P60, but not P30, KO neurons compared to WT (Fig. S2A, B). mEPSC amplitude was slightly but significantly reduced in P30, but not P60 KO neurons (Fig. S2A, C). These data suggest possible age- and brain region-dependent roles of CYLD.

To delineate the mechanism underlying enhanced hippocampal synaptic transmission, we examined the evoked EPSCs of Shaffer collateral-CA1 synapses. The paired-pulse ratios (PPRs), a measure of presynaptic release probability [42], were not significantly different at all intervals tested between KO and WT neurons (Fig. 2C), suggesting unaltered presynaptic mechanisms in mutant neurons. To further verify this, we performed a use-dependent NMDAR blockade assay with MK-801, an open-channel blocker of NMDARs. MK-801 more rapidly inhibits NMDARs at synapses with a high release probability, due to more frequent opening of these receptors, than those at low-release probability synapses. MK-801 had similar NMDAR-EPSC inhibition time courses in CYLD KO and WT neurons (Fig. 2D), confirming an intact glutamate release mechanism in mutant neurons. Finally, we examined the input-

output (I-O) relationship of AMPAR-EPSCs in response to increasing presynaptic stimulation intensities. EPSC amplitudes were markedly higher across all stimulus intensities in CYLD KO neurons compared to WT (Fig. 2E, F). Together, these results demonstrate that synaptic strength in CYLD KO mice is significantly increased, likely due to more functional synapses in mutant mice.

Augmented short-term but impaired long-term synaptic plasticity in CYLD KO mice
We next examined short- and long-term synaptic plasticity of Shaffer collateral-CA1 synapses (Fig. 3). Synaptic responses under current-clamp to high-frequency train stimulation allow assessment of summation and sustainment of postsynaptic depolarization at physiological firing frequencies [43]. WT neurons displayed a characteristic summation of postsynaptic depolarization in response to 15 20-Hz stimuli, which was significantly increased in CYLD KO neurons, suggesting enhanced short-term plasticity (Fig. 3A, B). Under voltage-clamp, NMDAR-dependent LTD induced by a standard low-frequency stimulation protocol (1000 pulses at 2 Hz) in WT (69.759 ± 5.6%) was absent in CYLD KO neurons (91.6 ± 9.0%; $p = 0.04$ vs. WT; two-tailed unpaired Student's t-test). In contrast, mGluR1-dependent LTD induced by the group I metabotropic glutamate receptor (mGluR1) agonist DHPG was similar in WT and KO neurons (Fig. 3E; $p = 0.47$ vs. WT; two-tailed unpaired Student's t-test). Finally, a conventional protocol involving pairing low-frequency (2 Hz) presynaptic stimulation with postsynaptic depolarization produced robust NMDAR-dependent LTP in WT (147.8 ± 13.4%); this LTP displayed a trend toward impairment in KO neurons (117.6 ± 15.8%; $p = 0.18$ vs. WT; two-tailed unpaired Student's t-test) (Fig. S3). Together, these results demonstrate that CYLD plays important roles in maintaining both short-term and NMDAR-dependent long-term synaptic plasticity.

CYLD promotes synapse pruning in a DUB-dependent manner
We next investigated synaptic alterations in CYLD KO mice at biochemical and structural levels and the roles of CYLD in
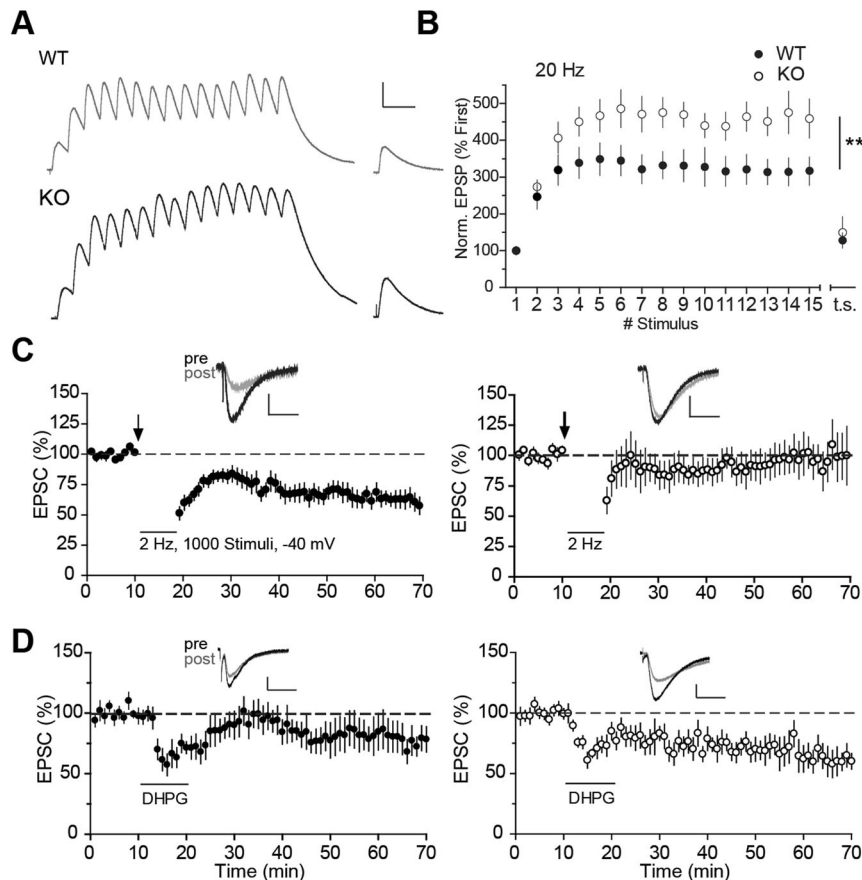
Fig. 3 Augmented short-term but impaired long-term synaptic plasticity in CYLD KO mice. A Synaptic summation as shown by representative EPSPs in response to a 15-pulse stimulus train at 20 Hz followed by a recovery test pulse. Scale bar: 5 mV, 100 ms. **B** Quantifications of synaptic summation from **A**, shown as summary of normalized EPSP amplitudes (to the peak of first EPSP) versus stimulus sequence during the train. $n = 9$ (WT) and 8 (KO) cells. **$p < 0.01$. Two-way ANOVA. **C** LTD induced (arrows) by 1000 stimuli at 2 Hz delivered to the Schaffer collateral afferent while holding CA1 cells at −40 mV. $n = 12$ (WT) and 7 (KO) cells. **D** mGluR1-LTD. DHPG (75 μM) was washed in between 10–20 min. $n = 7$ (WT) and 6 (KO) cells. Insets, representative EPSCs before (pre) and after (post) LTD induction. All LTD sample traces are averages of 5 EPSCs. Scale bars: 50 pA, 25 ms. Summary data are mean ± sem.

dendritic spine remodeling (Fig. 4). Immunoblotting (IB) analysis revealed significantly higher levels of hippocampal GluA1, GluN1, and PSD-95 in CYLD KO mice (Fig. 4A, B), consistent with increased postsynaptic efficacy. We then compared dendritic spine density of GFP-labeled neurons in P30 WT and KO mice by imaging CA1 hippocampal neurons injected on P15 with AAV2-hSyn-EGFP. KO neurons had a significant increase in numbers of total and mushroom (believed to be associated with mature, stable synapses [44]) spines (Fig. 4C, D). These data demonstrate that CYLD KO neurons possess excessive numbers of synapses.

To further investigate the causal role of CYLD in spine remodeling, we examined if CYLD overexpression can drive dendritic spine removal. Exogenous expression of CYLD in cultured rat hippocampal neurons resulted in significantly decreased total, mushroom, and stubby spine densities paralleled by an increase in filopodia protrusions (Fig. 4E, F), as well as significantly decreased GluA1 and GluN1 levels (Fig. S4). To distinguish whether CYLD-mediated spine removal was due to defective spine formation or facilitated spine pruning, we repeated above experiments in older neurons (Fig. 4G, H). Transfecting CYLD into neurons at DIV19, when the majority of synapses have been established and matured, still resulted in significant elimination of total and mushroom spines correlated with an increase of filopodia protrusions (Fig. 4G, H). Finally, to test if CYLD modulation of spines depended on its DUB activity, we expressed GFP control, wild-type CYLD, or a DUB-deficient CYLD

(C601A) mutant in cultured CYLD KO hippocampal neurons where endogenous CYLD was absent to eliminate potential confounding effects. We found that wild-type CYLD, but not the enzyme-dead C601A, significantly reduced total, mushroom, and stubby spine densities (Fig. 4I, J). Together, these results demonstrate that CYLD, in a DUB-dependent manner, drives pruning of existing glutamatergic synapses on mature neurons.

Impaired autophagy and hyperactive Akt-mTOR signaling in CYLD KO brains

We next investigated the mechanism by which CYLD drives synapse removal. We focused on autophagy because of its roles in synapse pruning [38, 41] and the potential links between CYLD and autophagy via K63 ubiquitination-related mechanisms [45–47]. There were significantly lower levels of LC3-II, the lipidated form of LC3-I and the only reliable marker for autophagosomes, and LC3-II/I ratio in KO hippocampal lysates at P30, P60, and P270 compared to WT (Fig. 5A, B). In addition, there was a significantly higher level of p62, an autophagy substrate and a functional readout of lysosomal degradation known to accumulate when autophagy is compromised, at all ages (Fig. 5A, B), supporting reduced autophagic flux in KO mice. LC3-I and LC3-II were also both significantly decreased in CYLD KO cortex (Fig. 5A, B). LC3 immunofluorescence showed significant reduction of LC3 puncta numbers in somas of CA1 neurons on hippocampal sections from KO mice, confirming reduced autophagosome formation (Fig. 5C, D). Finally, CYLD
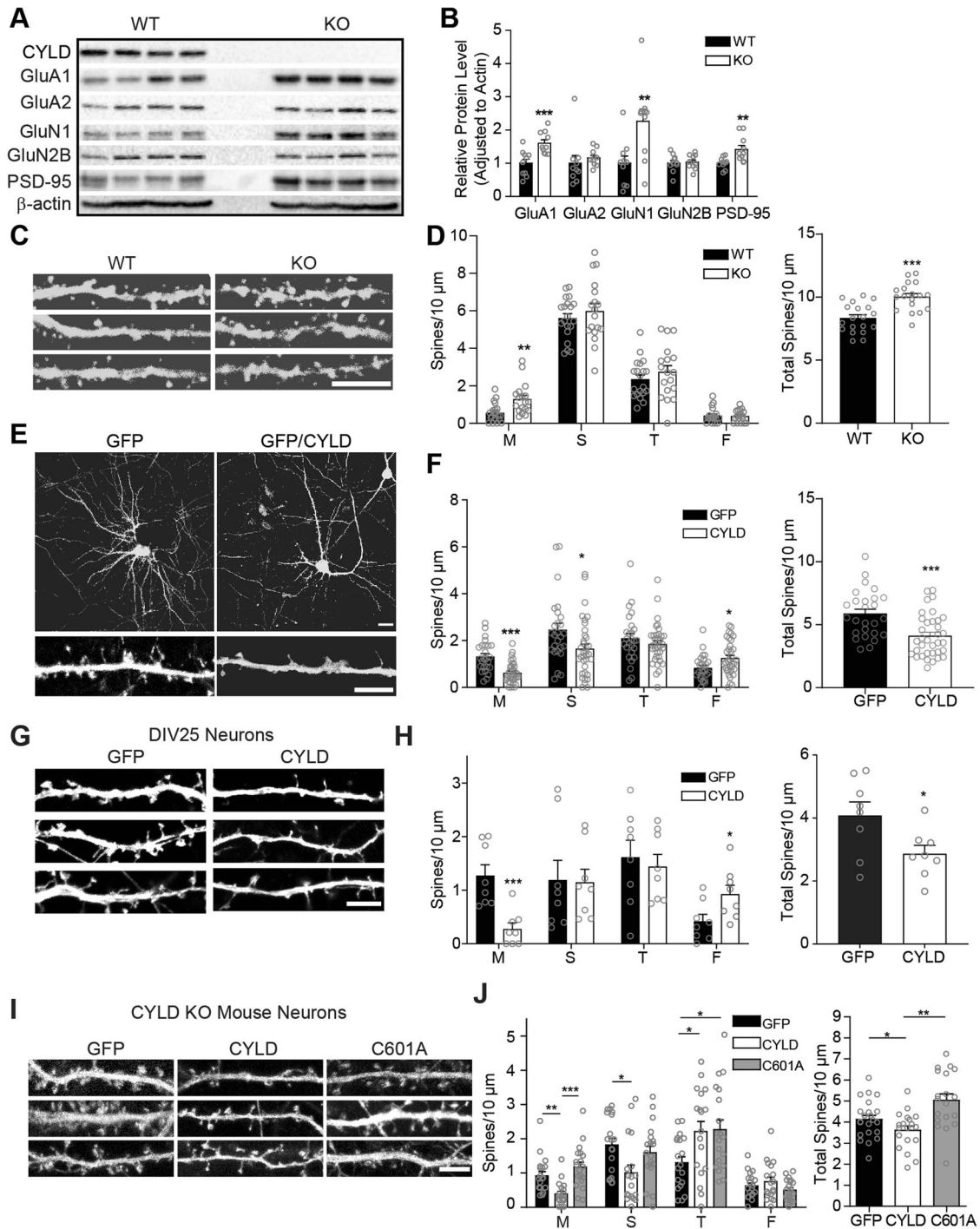
Fig. 4 CYLD promotes synapse pruning. A Representative blots of indicated synaptic proteins on CYLD WT and KO hippocampus lysates. **B** Quantification of protein levels from **A** normalized to WT controls. $n = 10$ (WT) and 10 (KO) mice. **C** Representative images of dendritic segments from AAV2-hSyn-EGFP infected CA1 hippocampal neurons. Scale bar: 5 μm. **D** Quantifications of dendritic spine density from **C**. $n = 20$ (WT) and 18 (KO) cells from 3 mice in each group. **E** Representative images of whole neurons (top) and dendritic segments (bottom) (DIV21) from GFP or GFP/CYLD transfected (DIV7) rat embryonic hippocampal neurons. Scale bars: 20 μm (top), 5 μm (bottom). **F** Quantifications of dendritic spine densities from **E**. $n = 26$ (GFP) and 35 (GFP/CYLD) cells from 3–4 independent cultures. **G, H** Effects of CYLD overexpression in mature neurons. Representative dendritic segments (**G**) and quantifications (**H**) from mature rat hippocampal neurons transfected with GFP or GFP/CYLD on DIV19 and imaged on DIV25. Scale bar: 5 μm. $n = 8$ (GFP) and 10 (GFP/CYLD) from 3 independent experiments. **I, J** Effects of CYLD and C601A in spine densities in cultured CYLD KO mouse neurons. Scale bar: 5 μm. $n = 21$ (GFP), 19 (CYLD), and 19 (C601A) cells. M, mushroom; S, stubby; T, thin; F, filopodia. $*p < 0.05$; $**p < 0.01$; $***p < 0.001$. Two-tailed unpaired t-tests or one-way ANOVA with post-hoc Bonferroni's multiple comparison test. Summary data are mean ± sem.
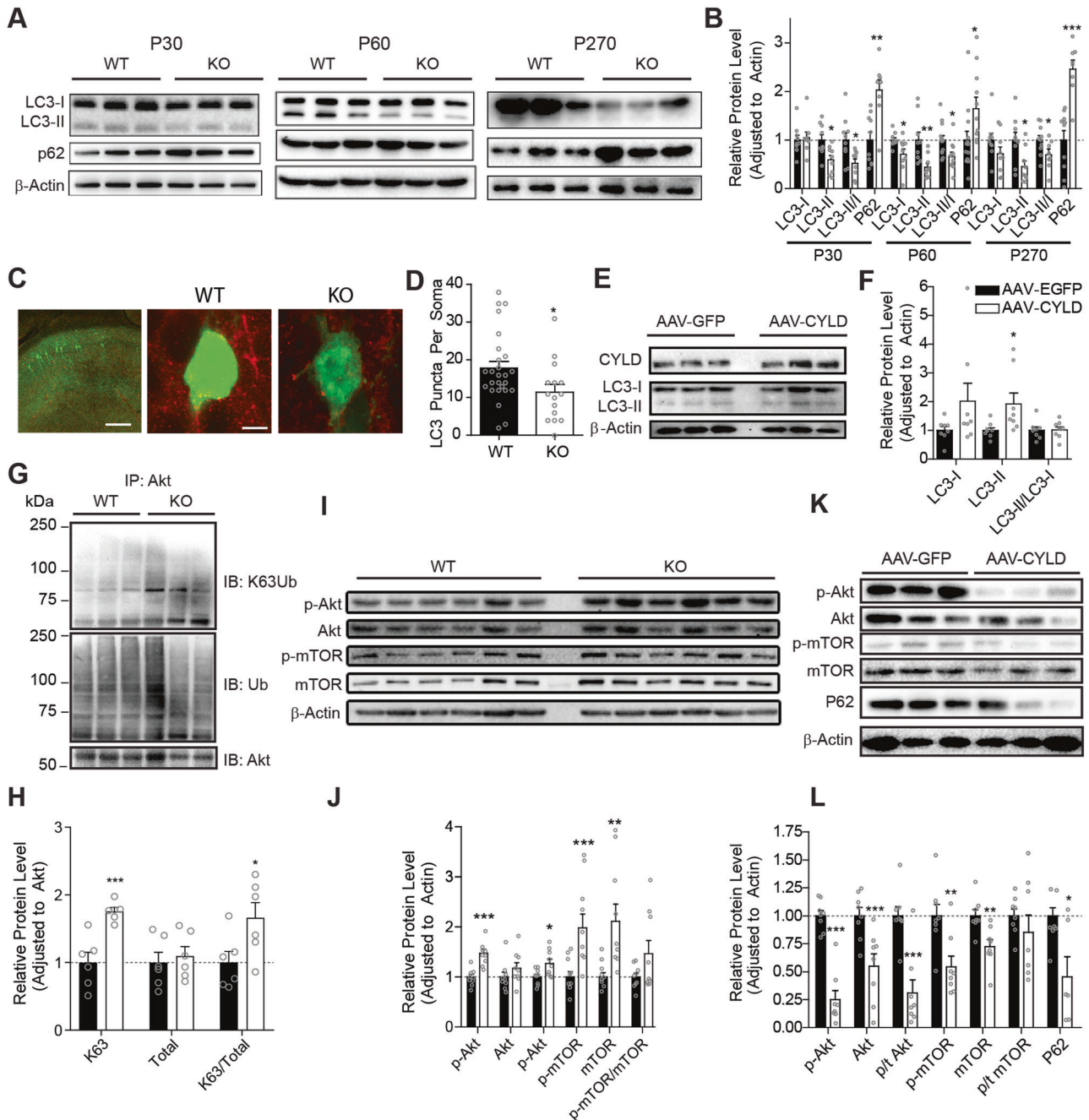
Fig. 5 Impaired autophagy and heightened Akt-mTOR signaling in CYLD KO hippocampus. A Representative LC3 and p62 blots on hippocampal lysates prepared from P30, P60, and P270 WT and CYLD KO mice. **B** Quantifications from **A**. Protein levels were first adjusted to β-actin and then normalized to respective WT levels. $n = 9$ (P30), 12 (P60), and 9 (P270) mice/group. **C** Representative LC3 staining on hippocampal sections from CYLD WT and KO brains injected with AAV2-hSyn-EGFP and stained for LC3 (red). Scale bars: 200 μm (left) and 5 μm (right). **D** Quantifications of LC3 puncta from **C**. LC3 puncta numbers per soma from WT and KO neurons infected with AAV-EGFP and stained for LC3 were quantified. $n = 26$ (WT) and 15 (KO) cells. **E** Representative LC3 blots on lysates prepared (DIV21) from cultured hippocampal neurons infected (DIV7) with AAV-EGFP or AAV-CYLD. **F** Quantifications of **E**. $n = 8$ mice/group. **G** Representative blots of K63-polyubiquitination (top) and total ubiquitination (bottom) of endogenous Akt in the mouse hippocampus. **H** Quantifications of **G**. $n = 6$ mice/group. **I** Representative total Akt, p-Akt (T308), total mTOR, p-mTOR (S2448), and β-actin blots on hippocampal lysates prepared from WT and CYLD KO mice. **J** Quantifications of **I**. $n = 9$ mice/group. **K** Representative blots on lysates prepared (DIV21) from cultured hippocampal neurons infected (DIV7) with AAV-EGFP or AAV-CYLD. **L** Quantifications of **K**. $n = 6$ mice/group for p62; $n = 8$ mice/group for all others. $*p < 0.05$, $**p < 0.01$, $***p < 0.001$. Two-tailed unpaired t-tests. Summary data are mean ± sem.

overexpression in cultured hippocampal neurons resulted in a significant increase in LC3-II (Fig. 5E, F), confirming that reduced autophagy in KO was due to a loss of CYLD. Together, these results demonstrate that CYLD promotes autophagy in neurons.

A master inhibitor of autophagy is mTOR, the catalytic subunit of the mTORC1 complex, which upon activation via phosphorylation at

S2448 inhibits the autophagy-initiating Ulk1 (Unc-51-like kinase) complex [48, 49]. Phospho-mTOR level was significantly elevated in both hippocampal (Fig. 5I, J) and cortical (Fig. S5C, D) lysates from CYLD KO, suggesting hyperactive mTOR in mutant brains. Akt/PKB, an upstream activator of mTOR [49, 50], undergoes K63-linked polyubiquitination that promotes its activation [51]. Akt is a direct

substrate of CYLD in non-neuronal cells, where CYLD directly deubiquitinates and inhibits Akt phosphorylation [8]. K63 ubiquitination of Akt, but not total Akt ubiquitination, was significantly increased in CYLD KO hippocampus (Fig. 5G, H), suggesting that Akt is also a substrate of CYLD in neurons. Consistently, we found a significant increase of phosphorylated (T308), but not total levels of Akt in CYLD KO hippocampal (Fig. 5I, J) and cortical (Figure S5C, D) lysates. Conversely, overexpressing CYLD in cultured hippocampal neurons produced a striking reduction of both total and phosphorylated levels of Akt and mTOR, accompanied with significantly reduced p62 (Fig. 5K, L). These results reveal an Akt-mTOR-autophagy signaling axis that is potently regulated by CYLD.

CYLD drives spine elimination in an autophagy-dependent manner

We next tested the hypothesis that CYLD drives spine pruning via autophagy in cultured neurons by treating with inhibitors that act at various steps along the autophagy pathway (Fig. 6). Consistent with above data, CYLD overexpression significantly reduced total, mushroom, stubby, and thin spines compared to DsRed-expressing control neurons (Fig. 6A–D). Treating cells with the Akt activator SC79, but not the vehicle control DMSO, did not affect spine densities in DsRed cells but prevented spine density reductions in CYLD-overexpressing neurons (Fig. 6A, B). Similar results were obtained with autophagy blockers Wortmannin and Bafilomycin A1, both blocking autophagosome-lysosome fusion, restoring total and mushroom spines to levels of DsRed/DMSO control (Fig. 6A, C, D). These data support that CYLD prunes synapses via an Akt- and autophagy activation-dependent mechanism.

Enhancing autophagy in CYLD KO rescues spine density, mEPSCs, and LTD

We finally examined if enhancing autophagy could restore the synaptic deficits in CYLD KO mice (Fig. 7). Mice were intraperitoneally administered rapamycin or saline daily from p20-p28 and sacrificed for assessments on p30 (Fig. 7A). For spine analysis, we also performed stereotaxic injections of AAV2-hSyn-EGFP to the CA1 hippocampus of WT and KO mice at P14/15 to label neurons (Fig. 7B), which was then followed by the rapamycin regimen. As expected, there was increased autophagy flux (with increasing LC3-II) and decreased GluA1 level in rapamycin-treated KO mice compared to saline controls (Fig. S6A, B). Rapamycin treatments (1.5 mg/kg) did not affect WT spine densities compared to saline, but restored mushroom and stubby spine densities in KO to WT control levels (Fig. 7C, D). Rapamycin at both low (1.5 mg/kg/day) and medium (3 mg/kg/day) doses also fully restored the enhanced mEPSC frequency in KO neurons to WT levels, where rapamycin did not have effects compared to saline (Fig. 7E, F; Fig. S6C). Rapamycin treatments did not affect mEPSC amplitude compared to saline under any conditions (Fig. 7E, F; Fig. S6D). Finally, rapamycin at 1.5/mg/kg also restored the lost LTD in KO mice to WT levels (Fig. 7G, H). Together, these results provide strong evidence that reduced autophagy in KO mice underlies their impaired spine density, synaptic strength, and LTD deficits.

DISCUSSION

In this study, we report that the FTD-linked K63 DUB CYLD is a critical regulator of synaptic maintenance and plasticity by acting on the Akt-mTOR-autophagy axis (Fig. 7I). We show that CYLD-deficient mice display aberrant locomotor, social, affective, and cognitive behaviors, accompanied with impaired synaptic numbers, efficacy, and plasticity. We further demonstrate that compromised neuronal autophagy resulting from heightened Akt-mTOR signaling underlies the synaptic function and plasticity deficits in mutant mice.

Based on its interactions with several autophagy receptors (i.e. p62/SQSTM1, Optineurin, and TBK1) [45, 46, 52] and HDAC6 [53], a protein that regulates autophagosome transport and maturation [54], CYLD is speculated to act as a "brake" on autophagy. Although mechanisms are unknown or unrelated, two recent studies support an inhibitory role for CYLD in autophagy in non-neuronal cells: CYLD has been shown to inhibit fusion of autophagosome with lysosome in HEK293 cells [17] and suppress autolysosome efflux in cardiomyocytes [55]. Our study reveals that CYLD enhances autophagy flux, consistent with a recent study [20], in the mouse hippocampus and cortex mediated by suppression of Akt and mTOR activity. This might be unexpected but not entirely surprising due to diverse CYLD interactors or substrates that can act on different nodes of the autophagy cycle differentially, which can further vary depending on cell types, subcellular compartments, and cargo types. Regardless of mechanism details, our results indicate that in intact brain, a net effect of CYLD is to facilitate autophagy flux.

In neurons, the autophagosome is believed to primarily form at the distal axon then is retrogradely transported along microtubules to the lysosome-enriched soma for degradation, and roles of autophagy in presynaptic functions such as neurotransmitter release and cargo degradations, have been extensively investigated [30, 33, 56]. In contrast, postsynaptic autophagy is less well studied [31, 33]. However, recent studies reveal the presence and activity-dependent trafficking of lysosomes as well as synaptic activity-regulated autophagic vacuole motility in dendrites and spines [57, 58]. Furthermore, postsynaptic (presumably) autophagy promotes developmental pruning of dendritic spine in the cortex [38], contributes to NMDAR-dependent LTD [34–36] in the hippocampus, and mediates BDNF-regulated synaptic plasticity and memory in response to nutritional stress [59]. Nevertheless, much of the molecular mechanisms in postsynaptic compartments remain elusive [31, 33]. Given that most CYLD localizes at postsynaptic sites and postsynaptic mechanisms mediate the synaptic strength and plasticity deficits in CYLD KO mice, our study uncovers a novel signaling mechanism, CYLD-Akt-mTOR, that regulates postsynaptic autophagy. However, potential roles of presynaptic CYLD in synaptic function and plasticity cannot be excluded.

Our results indicate that a physiological function of CYLD is to limit synapse strength and plasticity. CYLD promotes synapse elimination (but see [60]), likely by pruning/destabilizing existing spines from mature neurons in a DUB dependent manner rather than inhibiting synapse formation. Consistently, in the absence of CYLD, KO mice exhibit more abundant synapses, higher synaptic protein levels, and increased synaptic efficacy, likely in an age- and brain region-dependent manner. CYLD-deficient synapses also display impaired NMDAR-dependent LTD (and to a lesser degree, LTP) with intact mGluR1-LTD (presumably because mTOR activity is not compromised), suggesting that CYLD plays an important role in shaping synaptic properties and plasticity in addition to regulating synaptic density. Importantly, the spine morphology, mEPSC, and LTD deficits in CYLD mutant mice are rescued by restoring autophagy in vivo, supporting that decreased autophagy is behind these phenotypes. Overall, our results demonstrate that CYLD promotes synapse removal and mediates NMDAR-LTD via modulation of the Akt-mTOR signaling pathway through autophagy. However, it is worth noting that Akt-mTOR can also regulate synapse remodeling and plasticity via autophagy-independent mechanisms, e.g. mTOR-dependent protein translation [48, 61–63] and Akt-dependent synaptic GluA delivery [64], enhancement of which may counteract LTD in CYLD KO synapses. In addition, as no direct mechanistic link between autophagy and LTP has been reported, the somewhat impaired LTP in CYLD KO mice might be a consequence of saturated synaptic strength, which could occlude LTP. Finally, other CYLD substrates besides Akt, such as PSD-95 [14], β-catenin [65], and components in the NF-κB pathway [66–68], of which CYLD is a critical component [69, 70], can regulate synapse remodeling and plasticity.
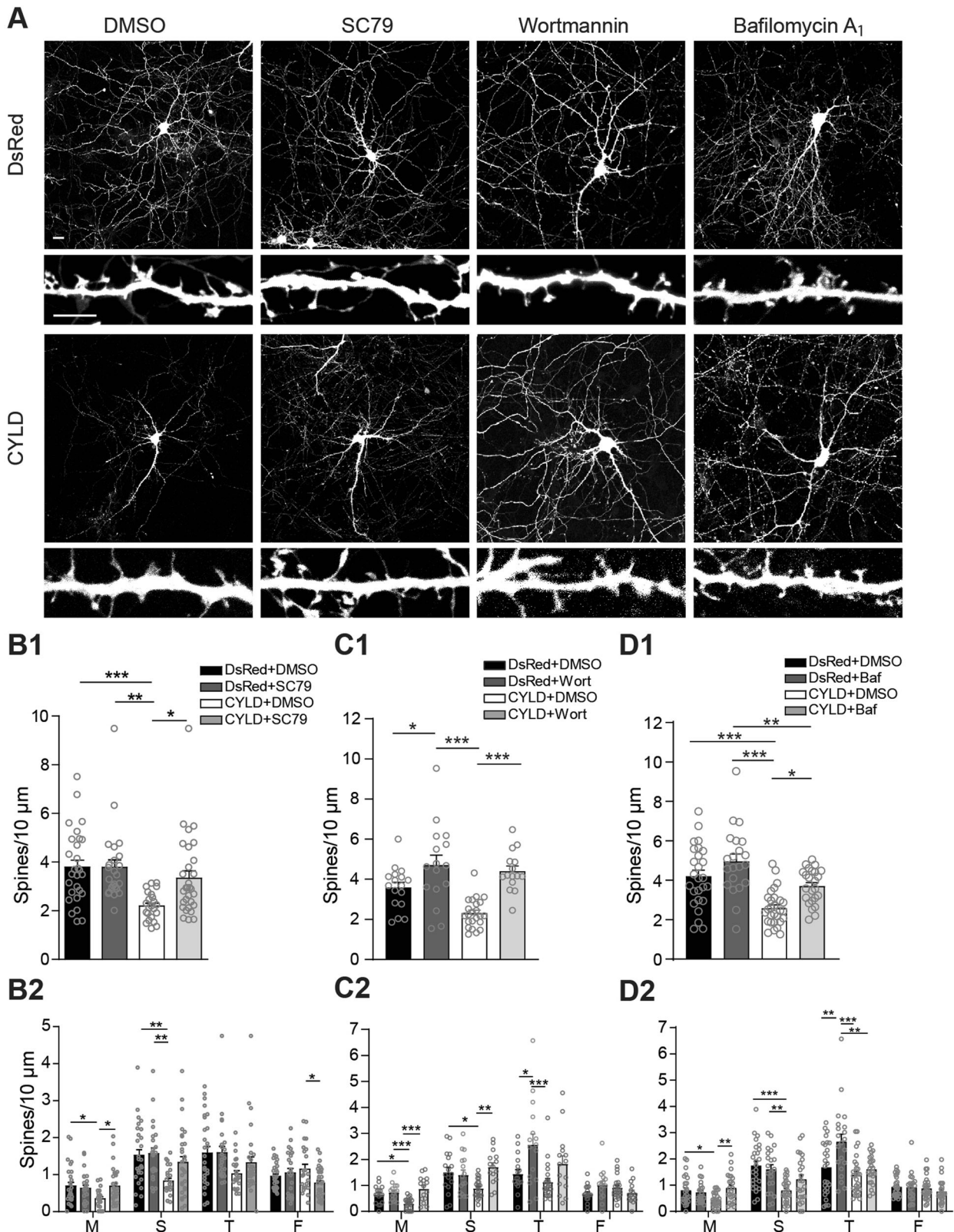
Fig. 6 CYLD drives spine elimination via Akt and autophagy. A Representative whole-neuron (top) and primary dendrite (bottom) images from cultured hippocampal neurons transfected with DsRed or DsRed/CYLD, and treated with either DMSO (vehicle), SC79 (15 μM), Wortmannin (100 nM) or Bafilomycin A$_1$ (10 nM) from DIV12–19. Scale bars: 20 and 5 μm. **B–D** Quantifications of SC79, Wortmannin (Wort), and Bafilomycin A1 (Baf) effects in spine densities. Total (B1, C1, and D1) and classified (B2, C2, and D2) spine densities are quantified from **A**. $n = 28$ (DsRed DMSO), 24 (DsRed SC79), 23 (CYLD DMSO), and 30 (CYLD SC79) cells; $n = 17$ (DsRed DMSO), 16 (DsRed Wort), 23 (CYLD DMSO), and 15 (CYLD Wort) cells; $n = 26$ (DsRed DMSO), 21 (DsRed Baf), 28 (CYLD DMSO), and 26 (CYLD Baf) cells. Cells were obtained from 3 independent experiments. $*p < 0.05$, $**p < 0.01$, $***p < 0.001$. One-way ANOVA with Bonferroni's multiple comparison post-hoc test. Summary data are mean ± sem.
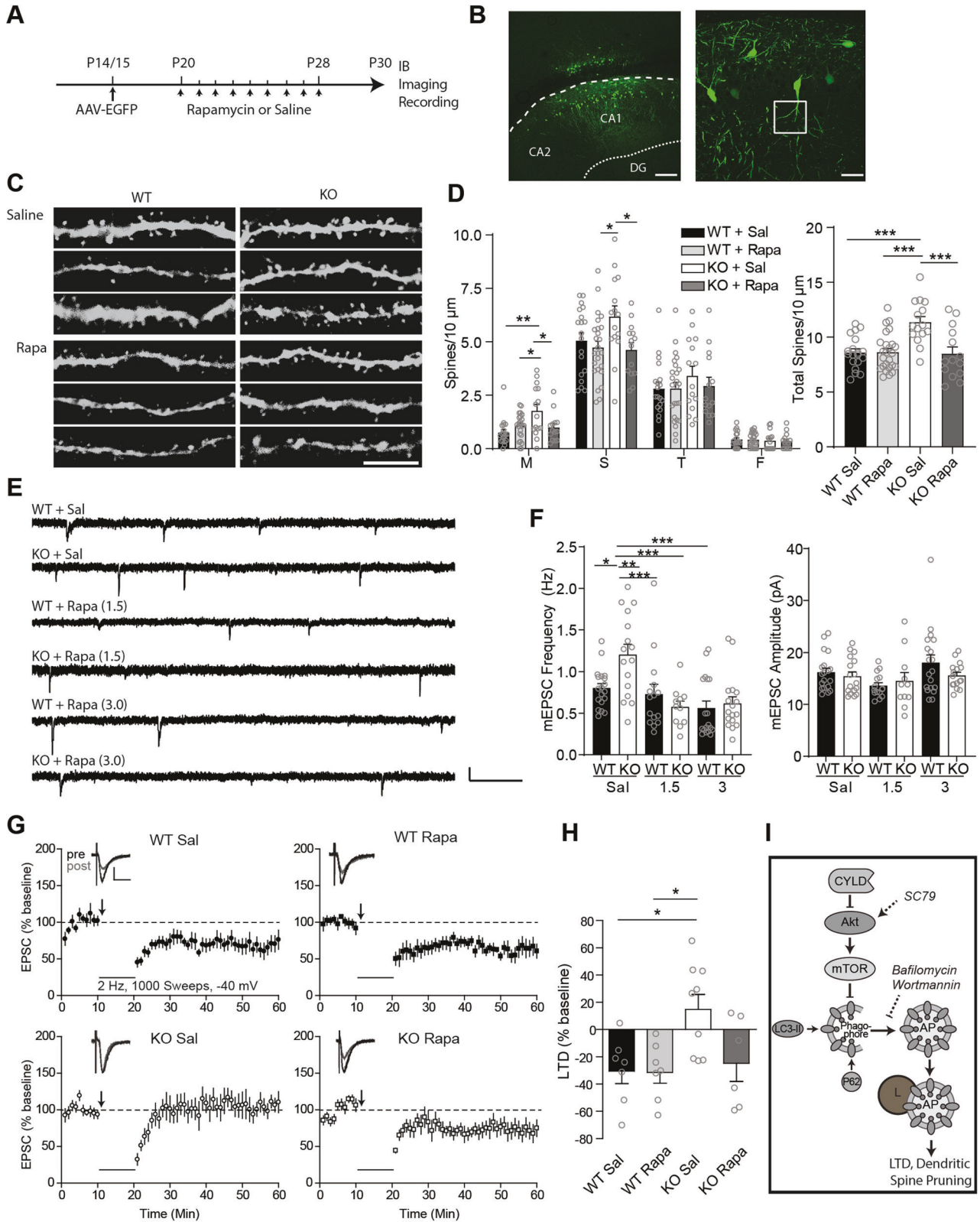
Nevertheless, these potential downstream mechanisms and the Akt-mTOR-autophagy mechanism identified here are not mutually exclusive in regulating synapse remodeling and plasticity.

Our study establishes that CYLD maintains an array of behaviors. Anxiety- and autism-like behaviors have been recently observed in CYLD deficient mice [19, 20]. Here we show that CYLD is critical in cognitive flexibility, as CYLD KO mice displayed deficits in a reversal learning task. This deficit can be explained at least partially by impaired LTD in mutant mice as hippocampal NMDAR-LTD is thought to mediate behavioral flexibility [71]. Whether the affective, social, and/or cognitive deficits in CYLD KO mice are mediated by altered mTOR-Akt-autophagy signaling remains to be determined.

Fig. 7 Rapamycin rescues spine density, synaptic efficacy, and LTD in CYLD KO mice. A Rapamycin treatment and analysis timeline. **B** Representative images showing AAV-EGFP infected neurons from a hippocampal slice. White box indicates the region of interest (first branch of the primary apical dendrite) for spine imaging. Scale bars: 200 µm (left) and 50 µm (right). **C** Representative dendritic segments from the first apical branch of CA1 hippocampal neurons prepared from CYLD WT and KO mice, treated with either saline or 1.5 mg/kg/day rapamycin. Scale bar: 5 µm. **D** Quantifications of spine densities from **C**. Sal, saline; Rapa, Rapamycin. $n = 19$ (WT Sal), 25 (WT Rapa), 15 (KO Sal), and 14 (KO Rapa) dendrites from 4–6 mice per group. **E** Representative mEPSC traces from CYLD WT and KO mice treated with saline, 1.5 mg/kg/day rapamycin, or 3 mg/kg/day rapamycin. Scale bar: 10 pA, 500 ms. **F** mEPSCs quantifications from **E**. $n = 19$ (WT Sal), 16 (KO Sal), 16 (WT Rapa 1.5), 11 (KO Rapa 1.5), 18 (WT Rapa 3), and 17 (KO Rapa 3) cells from 3–4 mice. **G** LTD rescue by rapamycin (1.5 mg/kg/day). Insets are representative EPSCs 5 min before (pre) and 40 min after (post) LTD induction. Scale bars: 50 pA, 25 ms. $n = 7$ (WT Sal), 7 (WT Rapa), 9 (KO Sal), and 6 (KO Rapa) cells. **H** LTD quantification, calculated from 20–40 min post-induction. **I** Working model. CYLD facilitates induction of neuronal autophagy via inhibition of Akt-mTOR, driving spine pruning and LTD. Dashed lines indicate the effect of different drugs used. AP, autophagosome; L, lysosome. $*p < 0.05$, $**p < 0.01$, $***p < 0.001$. One-way ANOVA with Bonferroni's multiple comparison post-hoc test. Summary data are mean ± sem.

Recently, three rare variants of the *CYLD* gene, predicted to have high pathogenic potentials, were identified in FTD/ALS patients, placing *CYLD* as the newest member of the FTD/ALS-causing gene family [17, 21]. FTD is characterized by striking changes in personality, social conduct, loss of empathy, apathy, anxiety, disinhibition, and language disability at early-mid stages, and general cognitive deteriorations at later stages [72], likely due to synaptic and circuit dysfunctions. Some of these FTD-related behaviors are impaired in CYLD KO mice. In addition, CYLD is a central regulator of immune signaling [69, 70], dysregulation of which is associated with many psychiatric and neurological diseases, which all involve synapse impairments and circuit mis-wiring [61, 73, 74]. Our findings thus provide a foundation for future investigation of synaptic and circuit deficits in neurological and psychiatric disease.

REFERENCES

1. Komander D, Lord CJ, Scheel H, Swift S, Hofmann K, Ashworth A, et al. The structure of the CYLD USP domain explains its specificity for Lys63-linked poly-ubiquitin and reveals a B box module. Mol Cell. 2008;29:451–64.
2. Bignell GR, Warren W, Seal S, Takahashi M, Rapley E, Barfoot R, et al. Identification of the familial cylindromatosis tumour-suppressor gene. Nat Genet. 2000;25:160–5.
3. Chen ZJ, Sun LJ. Nonproteolytic functions of ubiquitin in cell signaling. Mol Cell. 2009;33:275–86.
4. Husnjak K, Dikic I. Ubiquitin-binding proteins: decoders of ubiquitin-mediated cellular functions. Annu Rev Biochem. 2012;81:291–322.
5. Brummelkamp TR, Nijman SM, Dirac AM, Bernards R. Loss of the cylindromatosis tumour suppressor inhibits apoptosis by activating NF-kappaB. Nature. 2003;424:797–801.
6. Kovalenko A, Chable-Bessia C, Cantarella G, Israel A, Wallach D, Courtois G. The tumour suppressor CYLD negatively regulates NF-kappaB signalling by deubiquitination. Nature. 2003;424:801–5.
7. Trompouki E, Hatzivassiliou E, Tsichritzis T, Farmer H, Ashworth A, Mosialos G. CYLD is a deubiquitinating enzyme that negatively regulates NF-kappaB activation by TNFR family members. Nature. 2003;424:793–6.
8. Lim JH, Jono H, Komatsu K, Woo CH, Lee J, Miyata M, et al. CYLD negatively regulates transforming growth factor-beta-signalling via deubiquitinating Akt. Nat Commun. 2012;3:771.
9. Massoumi R, Chmielarska K, Hennecke K, Pfeifer A, Fassler R. Cyld inhibits tumor cell proliferation by blocking Bcl-3-dependent NF-kappaB signaling. Cell. 2006;125:665–77.
10. Reiley WW, Zhang M, Jin W, Losiewicz M, Donohue KB, Norbury CC, et al. Regulation of T cell development by the deubiquitinating enzyme CYLD. Nat Immunol. 2006;7:411–7.
11. Zhang J, Stirling B, Temmerman ST, Ma CA, Fuss IJ, Derry JM, et al. Impaired regulation of NF-kappaB and increased susceptibility to colitis-associated tumorigenesis in CYLD-deficient mice. J Clin Invest. 2006;116:3042–9.
12. Zajicek A, Yao WD. Remodeling without destruction: non-proteolytic ubiquitin chains in neural function and brain disorders. Mol Psychiatry. 2021;26:247–264.
13. Dosemeci A, Thein S, Yang Y, Reese TS, Tao-Cheng JH. CYLD, a deubiquitinase specific for lysine63-linked polyubiquitins, accumulates at the postsynaptic density in an activity-dependent manner. Biochem Biophys Res Commun. 2013;430:245–9.
14. Ma Q, Ruan H, Peng L, Zhang M, Gack MU, Yao WD. Proteasome-independent polyubiquitin linkage regulates synapse scaffolding, efficacy, and plasticity. Proc Natl Acad Sci USA. 2017;114:E8760–E8769.

15. Thein S, Tao-Cheng JH, Li Y, Bayer KU, Reese TS, Dosemeci A. CaMKII mediates recruitment and activation of the deubiquitinase CYLD at the postsynaptic density. PLoS ONE. 2014;9:e91312.
16. Jin C, Kim S, Kang H, Yun KN, Lee Y, Zhang Y, et al. Shank3 regulates striatal synaptic abundance of Cyld, a deubiquitinase specific for Lys63-linked poly-ubiquitin chains. J Neurochem. 2019;150:776–786.
17. Dobson-Stone C, Hallupp M, Shahheydari H, Ragagnin AMG, Chatterton Z, Carew-Jones F, et al. CYLD is a causative gene for frontotemporal dementia - amyotrophic lateral sclerosis. Brain. 2020;143:783–799.
18. Zhang J, Chen M, Li B, Lv B, Jin K, Zheng S, et al. Altered striatal rhythmic activity in cylindromatosis knock-out mice due to enhanced GABAergic inhibition. Neuropharmacology. 2016;110:260–267.
19. Han YY, Jin K, Pan QS, Li B, Wu ZQ, Gan L, et al. Microglial activation in the dorsal striatum participates in anxiety-like behavior in Cyld knockout mice. Brain Behav Immun. 2020;89:326–338.
20. Colombo E, Horta G, Roesler MK, Ihbe N, Chhabra S, Radyushkin K, et al. The K63 deubiquitinase CYLD modulates autism-like behaviors and hippocampal plasticity by regulating autophagy and mTOR signaling. Proc Natl Acad Sci USA. 2021;118:47.
21. Tabuas-Pereira M, Santana I, Kun-Rodrigues C, Bras J, Guerreiro R. CYLD variants in frontotemporal dementia associated with severe memory impairment in a Portuguese cohort. Brain. 2020.
22. Mizushima N, Komatsu M. Autophagy: renovation of cells and tissues. Cell. 2011;147:728–41.
23. Klionsky DJ. Autophagy: from phenomenology to molecular understanding in less than a decade. Nat Rev Mol Cell Biol. 2007;8:931–7.
24. Hara T, Nakamura K, Matsui M, Yamamoto A, Nakahara Y, Suzuki-Migishima R, et al. Suppression of basal autophagy in neural cells causes neurodegenerative disease in mice. Nature. 2006;441:885–9.
25. Komatsu M, Waguri S, Chiba T, Murata S, Iwata J, Tanida I, et al. Loss of autophagy in the central nervous system causes neurodegeneration in mice. Nature. 2006;441:880–4.
26. Nixon RA. The role of autophagy in neurodegenerative disease. Nat Med. 2013;19:983–97.
27. Yamamoto A, Yue Z. Autophagy and its normal and pathogenic states in the brain. Annu Rev Neurosci. 2014;37:55–78.
28. Menzies FM, Fleming A, Caricasole A, Bento CF, Andrews SP, Ashkenazi A, et al. Autophagy and neurodegeneration: pathogenic mechanisms and therapeutic opportunities. Neuron. 2017;93:1015–1034.
29. Gao FB, Almeida S, Lopez-Gonzalez R. Dysregulated molecular pathways in amyotrophic lateral sclerosis-frontotemporal dementia spectrum disorder. EMBO J. 2017;36:2931–2950.
30. Stavoe AKH, Holzbaur ELF. Autophagy in neurons. Annu Rev Cell Dev Biol. 2019;35:477–500.
31. Nikoletopoulou V, Tavernarakis N. Regulation and roles of autophagy at synapses. Trends Cell Biol. 2018;28:646–661.
32. Tomoda T, Yang K, Sawa A. Neuronal autophagy in synaptic functions and psychiatric disorders. Biol Psychiatry. 2020;87:787–796.
33. Lieberman OJ, Sulzer D. The synaptic autophagy cycle. J Mol Biol. 2020;432:2589–2604.
34. Shehata M, Matsumura H, Okubo-Suzuki R, Ohkawa N, Inokuchi K. Neuronal stimulation induces autophagy in hippocampal neurons that is involved in AMPA receptor degradation after chemical long-term depression. J Neurosci. 2012;32:10413–22.
35. Compans B, Camus C, Kallergi E, Sposini S, Martineau M, Butler C, et al. NMDAR-dependent long-term depression is associated with increased short term plasticity through autophagy mediated loss of PSD-95. Nat Commun. 2021;12:2849.
36. Shen H, Zhu H, Panja D, Gu Q, Li Z. Autophagy controls the induction and developmental decline of NMDAR-LTD through endocytic recycling. Nat Commun. 2020;11:2979.

37. Glatigny M, Moriceau S, Rivagorda M, Ramos-Brossier M, Nascimbeni AC, Lante F, et al. Autophagy is required for memory formation and reverses age-related memory decline. Curr Biol. 2019;29:435–448. e8.

38. Tang G, Gudsnuk K, Kuo SH, Cotrina ML, Rosoklija G, Sosunov A, et al. Loss of mTOR-dependent macroautophagy causes autistic-like synaptic pruning deficits. Neuron. 2014;83:1131–43.

39. Levine B, Kroemer G. SnapShot: macroautophagy. Cell. 2008;132:162. e1–162. e3.

40. Saxton RA, Sabatini DM. mTOR signaling in growth, metabolism, and disease. Cell. 2017;169:361–371.

41. Yan J, Porch MW, Court-Vazquez B, Bennett MVL, Zukin RS. Activation of autophagy rescues synaptic and cognitive deficits in fragile X mice. Proc Natl Acad Sci USA. 2018;115:E9707–E9716.

42. Zucker RS, Regehr WG. Short-term synaptic plasticity. Annu Rev Physiol. 2002;64:355–405.

43. Jakovcevski M, Ruan H, Shen EY, Dincer A, Javidfar B, Ma Q, et al. Neuronal Kmt2a/Mll1 histone methyltransferase is essential for prefrontal synaptic plasticity and working memory. J Neurosci. 2015;35:5097–108.

44. Kasai H, Matsuzaki M, Noguchi J, Yasumatsu N, Nakahara H. Structure-stability-function relationships of dendritic spines. Trends Neurosci. 2003;26:360–8.

45. Friedman CS, O'Donnell MA, Legarda-Addison D, Ng A, Cardenas WB, Yount JS, et al. The tumour suppressor CYLD is a negative regulator of RIG-I-mediated antiviral response. EMBO Rep. 2008;9:930–6.

46. Nagabhushana A, Bansal M, Swarup G. Optineurin is required for CYLD-dependent inhibition of TNFalpha-induced NF-kappaB activation. PLoS ONE. 2011;6:e17477.

47. Wooten MW, Geetha T, Babu JR, Seibenhener ML, Peng J, Cox N, et al. Essential role of sequestosome 1/p62 in regulating accumulation of Lys63-ubiquitinated proteins. J Biol Chem. 2008;283:6783–9.

48. Huber KM, Klann E, Costa-Mattioli M, Zukin RS. Dysregulation of mammalian target of rapamycin signaling in mouse models of autism. J Neurosci. 2015;35:13836–42.

49. Laplante M, Sabatini DM. mTOR signaling in growth control and disease. Cell. 2012;149:274–93.

50. Hay N, Sonenberg N. Upstream and downstream of mTOR. Genes Dev. 2004;18:1926–45.

51. Yang WL, Wang J, Chan CH, Lee SW, Campos AD, Lamothe B, et al. The E3 ligase TRAF6 regulates Akt ubiquitination and activation. Science. 2009;325:1134–8.

52. Jin W, Chang M, Paul EM, Babu G, Lee AJ, Reiley W, et al. Deubiquitinating enzyme CYLD negatively regulates RANK signaling and osteoclastogenesis in mice. J Clin Invest. 2008;118:1858–66.

53. Wickstrom SA, Masoumi KC, Khochbin S, Fassler R, Massoumi R. CYLD negatively regulates cell-cycle progression by inactivating HDAC6 and increasing the levels of acetylated tubulin. EMBO J. 2010;29:131–44.

54. Chin LS, Olzmann JA, Li L. Parkin-mediated ubiquitin signalling in aggresome formation and autophagy. Biochem Soc Trans. 2010;38:144–9.

55. Qi L, Zang H, Wu W, Nagarkatti P, Nagarkatti M, Liu Q, et al. CYLD exaggerates pressure overload-induced cardiomyopathy via suppressing autolysosome efflux in cardiomyocytes. J Mol Cell Cardiol. 2020;145:59–73.

56. Luningschror P, Sendtner M. Autophagy in the presynaptic compartment. Curr Opin Neurobiol. 2018;51:80–85.

57. Goo MS, Sancho L, Slepak N, Boassa D, Deerinck TJ, Ellisman MH, et al. Activity-dependent trafficking of lysosomes in dendrites and dendritic spines. J Cell Biol. 2017;216:2499–2513.

58. Kulkarni VV, Anand A, Herr JB, Miranda C, Vogel MC, Maday S. Synaptic activity controls autophagic vacuole motility and function in dendrites. J Cell Biol. 2021;220:6.

59. Nikoletopoulou V, Sidiropoulou K, Kallergi E, Dalezios Y, Tavernarakis N. Modulation of autophagy by BDNF underlies synaptic plasticity. Cell Metab. 2017;26:230–242. e5.

60. Li J, Sekine-Aizawa Y, Ebrahimi S, Tanaka S, Okabe S. Tumor suppressor protein CYLD regulates morphogenesis of dendrites and spines. Eur J Neurosci. 2019;50:2722–2739.

61. Estes ML, McAllister AK. Immune mediators in the brain and peripheral tissues in autism spectrum disorder. Nat Rev Neurosci. 2015;16:469–86.

62. Borrie SC, Brems H, Legius E, Bagni C. Cognitive dysfunctions in intellectual disabilities: the contributions of the Ras-MAPK and PI3K-AKT-mTOR pathways. Annu Rev Genomics Hum Genet. 2017;18:115–142.

63. Richter JD, Bassell GJ, Klann E. Dysregulation and restoration of translational homeostasis in fragile X syndrome. Nat Rev Neurosci. 2015;16:595–605.

64. Hu H, Qin Y, Bochorishvili G, Zhu Y, van Aelst L, Zhu JJ. Ras signaling mechanisms underlying impaired GluR1-dependent plasticity associated with fragile X syndrome. J Neurosci. 2008;28:7847–62.

65. Tauriello DV, Haegebarth A, Kuper I, Edelmann MJ, Henraat M, Canninga-van Dijk MR, et al. Loss of the tumor suppressor CYLD enhances Wnt/beta-catenin signaling through K63-linked ubiquitination of Dvl. Mol Cell. 2010;37:607–19.

66. Kaltschmidt B, Kaltschmidt C. NF-kappaB in the nervous system. Cold Spring Harb Perspect Biol. 2009;1:a001271.

67. Meffert MK, Baltimore D. Physiological functions for brain NF-kappaB. Trends Neurosci. 2005;28:37–43.

68. Mei S, Ruan H, Ma Q, Yao WD. The ubiquitin-editing enzyme A20 regulates synapse remodeling and efficacy. Brain Res. 2020;1727:146569.

69. Komander D, Clague MJ, Urbe S. Breaking the chains: structure and function of the deubiquitinases. Nat Rev Mol Cell Biol. 2009;10:550–63.

70. Sun SC. Deubiquitylation and regulation of the immune response. Nat Rev Immunol. 2008;8:501–11.

71. Collingridge GL, Peineau S, Howland JG, Wang YT. Long-term depression in the CNS. Nat Rev Neurosci. 2010;11:459–73.

72. Neary D, Snowden JS, Gustafson L, Passant U, Stuss D, Black S, et al. Fronto-temporal lobar degeneration: a consensus on clinical diagnostic criteria. Neurology. 1998;51:1546–54.

73. Boulanger LM, Shatz CJ. Immune signalling in neural development, synaptic plasticity and disease. Nat Rev Neurosci. 2004;5:521–31.

74. Hammond TR, Marsh SE, Stevens B. Immune signaling in neurodegeneration. Immunity. 2019;50:955–974.

AUTHOR CONTRIBUTIONS

A.S.Z., H.R. and W.-D.Y. designed research; A.S.Z., H.R., H.D., M.C.M., H.L.P., W.J.B. and B.J. performed research; S.C.S. contributed reagents; A.S.Z, H.R., H.D., M.C.S., H.L.P., W.J.B., B.J., S.A. and W.-D.Y. analyzed data; and A.S.Z., H.R. and W.-D.Y. wrote the paper.

COMPETING INTERESTS

The authors declare no conflict of interest.

ADDITIONAL INFORMATION

Supplementary information The online version contains supplementary material available at https://doi.org/10.1038/s41380-022-01571-1.

Correspondence and requests for materials should be addressed to Wei-Dong Yao.

Reprints and permission information is available at http://www.nature.com/reprints

Publisher's note Springer Nature remains neutral with regard to jurisdictional claims in published maps and institutional affiliations.